



## Article

# Monitoring the Dissipation of the Floating Green Macroalgae Blooms in the Yellow Sea (2007–2020) on the Basis of Satellite Remote Sensing

Deyu An <sup>1,2</sup>, Dingfeng Yu <sup>1,2</sup>, Xiangyang Zheng <sup>2,3</sup>, Yan Zhou <sup>1</sup> , Ling Meng <sup>2,3</sup> and Qianguo Xing <sup>2,3,4,\*</sup>

<sup>1</sup> Institute of Oceanographic Instrumentation, Qilu University of Technology (Shandong Academy of Sciences), Qingdao 266001, China; dyan@qlu.edu.cn (D.A.); dfyu@qlu.edu.cn (D.Y.); zhouyan\_ocrs@qlu.edu.cn (Y.Z.)

<sup>2</sup> CAS Key Laboratory of Coastal Environmental Processes and Ecological Remediation, Yantai Institute of Coastal Zone Research, Chinese Academy of Sciences, Yantai 264003, China; xyzheng@yic.ac.cn (X.Z.); lmeng@yic.ac.cn (L.M.)

<sup>3</sup> University of Chinese Academy of Sciences, Beijing 100049, China

<sup>4</sup> Center for Ocean Mega-Science, Chinese Academy of Sciences, Qingdao 266071, China

\* Correspondence: qgxing@yic.ac.cn

**Abstract:** Large scale green macroalgae blooms (MABs) caused by *Ulva prolifera* have occurred regularly in the Yellow Sea since 2007. In the MAB dissipation phase, the landing or sinking and decomposition of *U. prolifera* would alter the physical-chemical environment of seawater and cause ecological, environmental, and economic problems. To understand MAB dissipation features, we used multiple sensors to analyze the spatiotemporal variation of the MAB dissipation phase in the southern Yellow Sea. The results show the variation in the daily dissipation rate (DR) was inconsistent from year to year. Based on the DR variation, a simple method of estimating MAB dissipation days was proposed for the first time. Verification results of the method, from 2018 to 2020, showed the estimated dissipation days were relatively consistent with the results obtained by remote sensing imagery. From 2007 to 2020, the order in which macroalgae landed in the coastal cities of Shandong Peninsula can be roughly divided into two types. In one type, the macroalgae landed first in Rizhao, followed by Qingdao, Rushan, and Haiyang. In the other type, they landed in the reverse order. The MABs annual distribution density showed significant differences in the southern Yellow Sea. These results provided a basis for evaluating the MABs' impact on marine ecology and formulating the green-tide prevention and control strategies.

**Keywords:** macroalgae blooms; spatiotemporal variation; dissipation phase; the southern Yellow Sea; multiple sensors



**Citation:** An, D.; Yu, D.; Zheng, X.; Zhou, Y.; Meng, L.; Xing, Q. Monitoring the Dissipation of the Floating Green Macroalgae Blooms in the Yellow Sea (2007–2020) on the Basis of Satellite Remote Sensing. *Remote Sens.* **2021**, *13*, 3811. <https://doi.org/10.3390/rs13193811>

Academic Editors: Weizeng Shao, Juhong Zou, Ferdinando Nunziata and Gang Zheng

Received: 16 August 2021

Accepted: 17 September 2021

Published: 23 September 2021

**Publisher's Note:** MDPI stays neutral with regard to jurisdictional claims in published maps and institutional affiliations.



**Copyright:** © 2021 by the authors. Licensee MDPI, Basel, Switzerland. This article is an open access article distributed under the terms and conditions of the Creative Commons Attribution (CC BY) license (<https://creativecommons.org/licenses/by/4.0/>).

## 1. Introduction

Macroalgal blooms (MABs), caused by the outbreak of macroalgae, have increased remarkably in the global oceans in recent years and have become a worldwide marine ecological problem [1–4]. The world's largest MABs of *Ulva prolifera* (“green tide”) have occurred every summer in the Yellow Sea since 2007, causing serious ecological, environmental, and socioeconomic problems [5,6]. Scholars at home and abroad have conducted a lot of research on green tide, mostly concentrated on remote sensing monitoring methods [7–9], sub-pixel coverage area estimation methods [10,11], origin [12–14], evolution process [15,16] and driving mechanisms [17–19], etc., and they have achieved good results. At present, the remote sensing monitoring methods of the green tide are basically mature and the overall understanding and the early development processes are largely clear: many studies from multiple perspectives including satellite remote sensing, ocean circulation models, and field observations indicate that *U. prolifera* originates in the Subei Shoal of Jiangsu Province [20–25], which is related to the increased cultivation of seaweed

(*Porphyra yezoensis*) in this area [14,22]. Evidence has indicated that *P. yezoensis* aquaculture rafts would be the main source of *U. prolifera* [13,22,26–28]. Every April, when mariculture rafts were recycled after harvesting the seaweed *P. yezoensis*, *U. prolifera* macroalgae attached to the rafts were scraped off and discarded into sea water [14,22,29]. These discarded macroalgae grew rapidly and developed into large-scale MABs in June and July under favorable sunlight, temperature, and nutrient conditions [6,22,30]. They moved toward the Shandong Peninsula following the southeast monsoon and summer ocean surface currents [31].

Green tide significantly altered the offshore chlorophyll concentration (an index of phytoplankton biomass) and the Secchi Disk Depth (a proxy of water clarity) in the Yellow Sea [32,33] during the blooms. In the MAB dissipation phase, large amounts of *U. prolifera* either aggregated in the Shandong Peninsula coastal water and sank into the sea or landed on the Shandong Peninsular coasts. During *U. prolifera* decomposition, large amounts of nutrients were released into the sea, which altered the physico-chemical environment of the sea water. Some toxic substances such as  $H_2S$  were also released, affecting the growth of shellfish and other organisms, threatening the sustainable development of aquaculture, and endangering the marine ecological security in coastal areas [34,35]. In addition, the landing of *U. prolifera* leads to serious impacts on the landscape, ecological environment, and human activities, causing serious socioeconomic losses [22,36]. In short, MABs have a serious ecological and socioeconomic impact in the MAB dissipation phase, on the Shandong Peninsular coasts. Thus, understanding the MAB dissipation phase is essential for effectively controlling such impacts.

Since MODIS and Landsat first detected large-scale green tide in 2007 [12,13], the Yellow Sea has consistently produced the world's largest green tide bloom every summer from 2007–2020. When and where was the green tide dissipated in these years? Is there a rule to follow? Answering to these questions is very important for further assessing the impacts of the green tide. Therefore, we selected the main distribution region of MABs since 2007, in the Yellow Sea (Figure 1), as our study area and used multiple sensors to systematically analyze spatiotemporal variation in the dissipation process of the MABs.

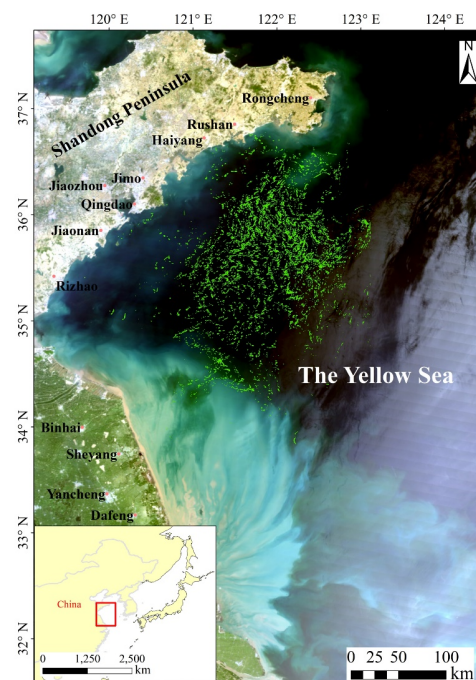


**Figure 1.** The study area. The background image is MODIS true color image on 6 May 2009, in which the green slicks show the *U. prolifera* macroalgae bloom in 2009.

## 2. Data and Methods

### 2.1. Study Area

The Yellow Sea is a marginal sea in the western Pacific Ocean, located between the Chinese mainland and the Korean Peninsula (31°40'N~39°50'N, 119°10'E~126°50'E), and is a semi-enclosed shallow sea. The Yellow Sea is usually divided into two parts of the north and the south, based on the connection between Chengshantou on the Shandong Peninsula and Changshan on the Korean Peninsula. The area of the North Yellow Sea is  $7.1 \times 10^4$  km<sup>2</sup>. The area of the South Yellow Sea is  $30.9 \times 10^4$  km<sup>2</sup>, which is the main area that green tides have broken out in recent years. According to the main areas of green tide outbreaks since 2008, the study area is within the range of 31°32'N~37°25'N, 119°7'E~123°3'E in the South Yellow Sea (Figure 1).

### 2.2. Remote Sensing Images, Data Processing, and MABs Area Statistics

Satellite images with low cloud coverage over the Yellow Sea were acquired for May–August of 2007–2020 and were used to identify MABs. Considering the temporal and spatial resolution of the remote sensing image and the patch area distribution at different development stages of the green tide, the level 1 imagery selected were the Terra and Aqua Moderate Resolution Imaging Spectrometer (MODIS), Huanjing-1A/1B (HJ-1A/1B), GaoFen-1(GF-1), and Sentinel-2 A/B. The spatial resolutions of MODIS, HJ-1A/1B, GF-1, and Sentinel-2 were 250, 30, 16, and 10 m, respectively. Based on the macroalgal-aggregation morphology at different stages of MABs and their spatial resolutions, the MODIS images were used to identify the MABs, and the HJ-1A/1B, GF-1, and Sentinel-2 images were used as supplementary information to precisely locate small patches of macroalgae that might be missed in MODIS images.

The images were processed with georeferencing and atmospheric corrections. The FLAASH (Fast Line of Sight Atmospheric Analysis of Spectral Hypercubes) atmospheric correction module via ENVI 5.3 software (Exelis Visual Information Solutions, Inc., Boulder, CO, USA) was applied to MODIS, HJ-1A/1B, and GF-1 images to derive the reflectance ( $R$ , unitless), while the Sen2Cor atmospheric correction module from European Space Agency was used on the Sentinel-2 images. All images are transformed into WGS\_1984\_UTM\_Zone\_51N coordinate system after projection.

Based on the distinct spectral difference between natural seawater and macroalgae-covered seawater, scholars at home and abroad have proposed many macroalgae information detection algorithms. Among them, the difference index algorithm, such as Floating Algae Index (FAI), Difference Vegetation Index ( $DVI$ ), Virtual-Baseline Floating macroalgae Height (VB-FAH), is less sensitive to the effects of sunlight and aerosol changes [9,28]. Since MODIS 250 m images only have two bands of red light (Red) and near-infrared (NIR), the  $DVI$  index (Equation (1)) is selected for macroalgae pixels' extraction.

$$DVI = R_{NIR} - R_{Red}, \quad (1)$$

where  $R_{NIR}$  is the reflectance at the near-infrared (NIR) band and  $R_{Red}$  is the Red band reflectance.

Given the significant variability in atmospheric turbidity, ocean background, and sun glint [9,37], a dynamic threshold of  $DVI$  was used to extract the macroalgae. The  $DVI$  images were segmented into several small windows, and the threshold of each window is determined according to the difference between green macroalgae and seawater background, and then the macroalgae pixels in each window are extracted in turn [9,28]. The daily coverage area of MABs ( $A_T$ , km<sup>2</sup>) was derived by multiplying the pixel size of the satellite image ( $PS$ , in km<sup>2</sup>) by the total number of pixels ( $N$ ) identified as macroalgae [28,37], as shown in Equation (2).

$$A_T = PS \times N, \quad (2)$$

Image pairs over the same macroalgae region with the same acquisition dates were selected to investigate the consistency in the retrieved macroalgae coverage area [14]. The

areas derived from different image pairs were then compared. Two linear regression ( $R^2 > 0.921$ ) fits as cross-calibration of  $A_T$  among the fine spatial resolution sensors. Based on two linear regression functions, the results of Sentinel-2 and HJ-1A/1B images were converted the results to the resolution level of GF-1 (Figure 2a). Three linear regression functions ( $R^2 > 0.823$ ) were performed on the areas derived from Sentinel-2, HJ-1A/1B, and GF-1 images and the areas derived from MODIS. On the basis, the results of Sentinel-2, HJ-1A/1B images and GF were converted the results to the resolution level of MODIS (Figure 2b).

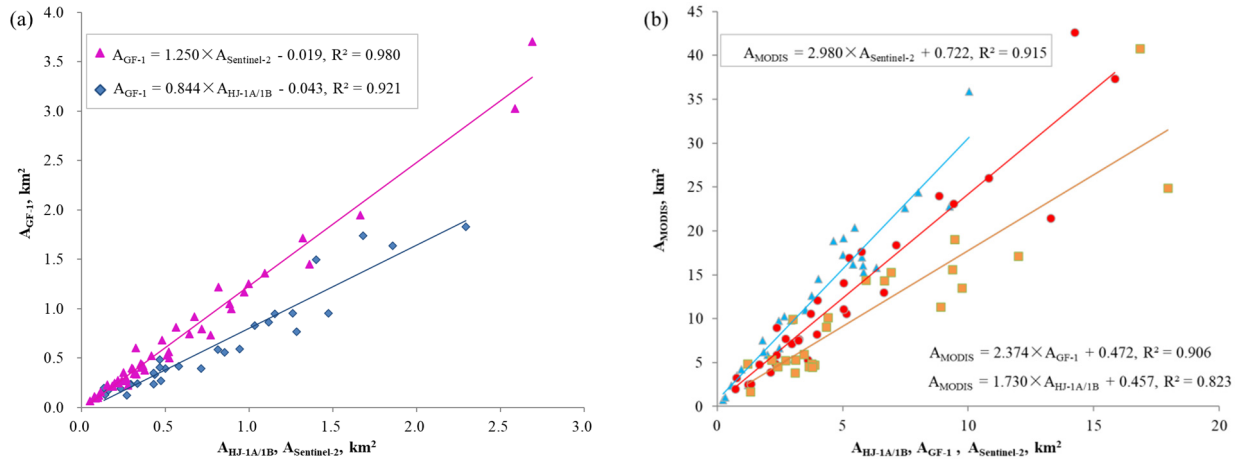


**Figure 2.** (a) Comparison in the macroalgae coverage areas derived from the optical images of HJ-1A/1B, GF-1 and Sentinel-2, i.e.,  $A_{HJ-1A/1B}$ ,  $A_{GF-1}$ ,  $A_{Sentinel-2}$ , respectively. (b) Comparison in the macroalgae coverage areas derived from the optical images of MODIS, HJ-1A/1B, GF-1 and Sentinel-2, i.e.,  $A_{MODIS}$ ,  $A_{HJ-1A/1B}$ ,  $A_{GF-1}$ ,  $A_{Sentinel-2}$ , respectively.

### 2.3. Calculation and Analysis of Macroalgae Daily Dissipation Rate

We used the extracted data on floating macroalgal cover to define two dissipation metrics, the days from maximum cover to bloom-free condition (dissipation days), and the rate at which the bloom declined between observations (dissipation rate). For the first, for each year we determine the maximum daily coverage area ( $A_{MAX}$ ) and the minimum daily coverage area ( $A_{MIN}$ ).  $A_{MAX}$  is the maximum of  $A_T$  extracted by remote sensing images every year.  $A_{MIN}$  is defined according to the distribution of the study area. In this study, when  $A_T$  is less than 0.01% of the distribution area (about  $1.6 \times 10^5 \text{ km}^2$ ) of the study region, i.e.,  $A_T \leq 16 \text{ km}^2$ , it is regarded as  $A_{MIN}$ . At this time, MABs enter the end of the dissipation phase, indicating that the MABs event is coming to an end for that year. The dissipation days is the time taken to reduce  $A_{MAX}$  to  $A_{MIN}$ . Then, the DR of the MAB dissipation phase is then calculated using Equation (3).

$$DR = 1 - \left( \frac{A_j}{A_i} \right)^{\frac{1}{j-i}}, \quad (3)$$

where  $i, j$  is the day of the year, and  $j$  is later than  $i$ ;  $A$  is the  $A_T$  included  $A_{MODIS}$  and  $A_{GF}$  or the sub-pixel coverage area of MABs ( $A_{CCM}$ ), and the  $A_{CCM}$  statistical of the fine resolution images in this study is based on sub-pixel coverage model proposed by Li et al. (2018) [10]. It was built on the assumptions of a pure pixel of the floating macroalgae on the remote sensing image, normalizing the  $DVI$  values of all the macroalgae pixels ([01DVI]) firstly (Equation (4)), and then calculating the  $POM$  in each macroalgae pixel (Equation (5)) and  $A_{CCM}$  (Equation (6)).

$$[01DVI] = (DVI - DVI_{min}) / (DVI_{max} - DVI_{min}), \quad (4)$$

$$POM = 0.973 \times [01DVI] + 0.027, \quad (5)$$

$$A_{CCM} = \sum_{i=1}^n POM_i \times P_i \quad (6)$$

In this study, two characteristics were selected to systematically analyze *DR* variation in MAB dissipation. One is the macroalgae daily dissipation rate (*DR*) in a period between every two neighboring dates (TND), and the other is the *DR* calculated during the periods from the same starting date to different ending dates (DSE).

To further determine the variables ( $A_T$  or  $A_{CCM}$ ) used to calculate *DR*, the results extracted by remote sensing images in 2018 were used to investigate the consistency in the *DR* calculated by  $A_T$  and  $A_{CCM}$ . The *DR* calculated by  $A_T$  and  $A_{CCM}$  has a good correlation with a mean relative difference of less than 16.40% (Figure 3a,b). The reason for this is that there is a significant correlation between  $A_{GF}$  and  $A_{CCM}$  ( $R^2 = 0.991$ , Figure 3c) and between  $A_{GF}$  and  $A_{MODIS}$  ( $R^2 = 0.906$ , Figure 2b). Equation (3) is a ratio equation, which can reduce the gain deviation between  $A_T$  and  $A_{CCM}$ . Because of MODIS' superior temporal resolution, the *DR* calculated by  $A_{MODIS}$  was selected to analyze the *DR* variation.

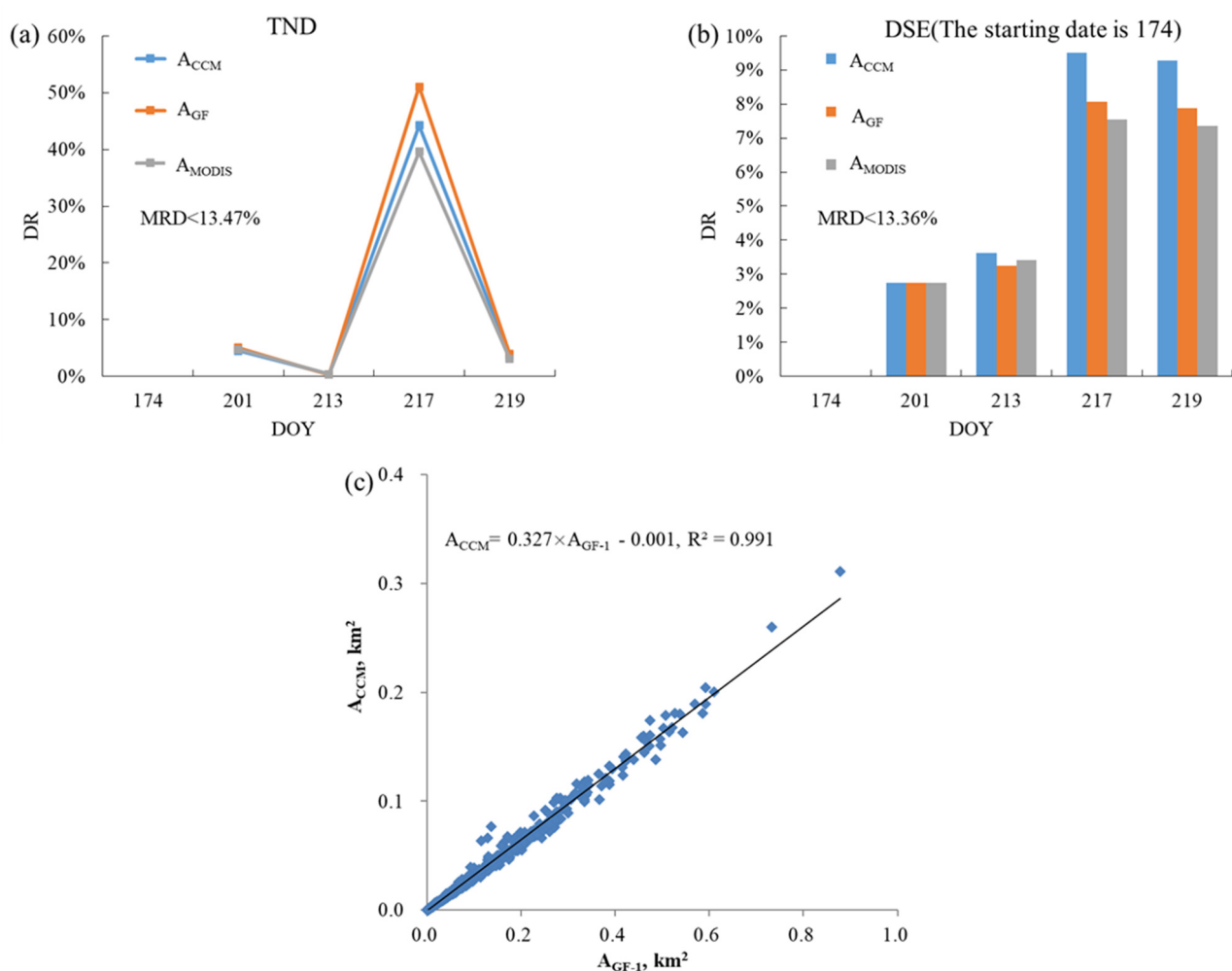


**Figure 3.** Consistency analysis of the daily dissipation rate (*DR*) calculated by  $A_T$  and  $A_{CCM}$ . (a) The *DR* in a period between every two neighboring dates (TND). (b) The *DR* calculated during the periods from the same starting date (i) to different ending dates (DSE). (c) Comparison of the macroalgae coverage area and the sub-pixel coverage, i.e.,  $A_{GF-1}$  and  $A_{CCM}$ , respectively.

#### 2.4. Analysis of the Spatiotemporal Variation in MABs Dissipation

Two characteristics were selected to systematically analyze spatiotemporal variation in MAB dissipation. One was the location order in which the macroalgae landed in the coastal cities of Shandong Peninsula (LLO) to study the change characteristics of the landing

location during the dissipation phase of the green tide. Results from 2008 were used as an example to show the LLO determination process. First, the location of the first landing in a coastal city was predicted based on the MABs monitoring results from the remote sensing images. In 2008, this occurred between June 5 and June 29 (Figure 4a). Next, based on the daily distribution of the MABs, the location of minimum distance from offshore (LMD) was extracted using the Near module in Analysis Tools of ArcGIS software. Note that the subminimum distance was extracted if the next LMD was the same as the previous one (Figure 4b). Third, a geometric union of LMD was computed in ArcGIS software. Finally, the LLO was determined by the Point-to-Line module in ArcGIS software (Figure 4c).

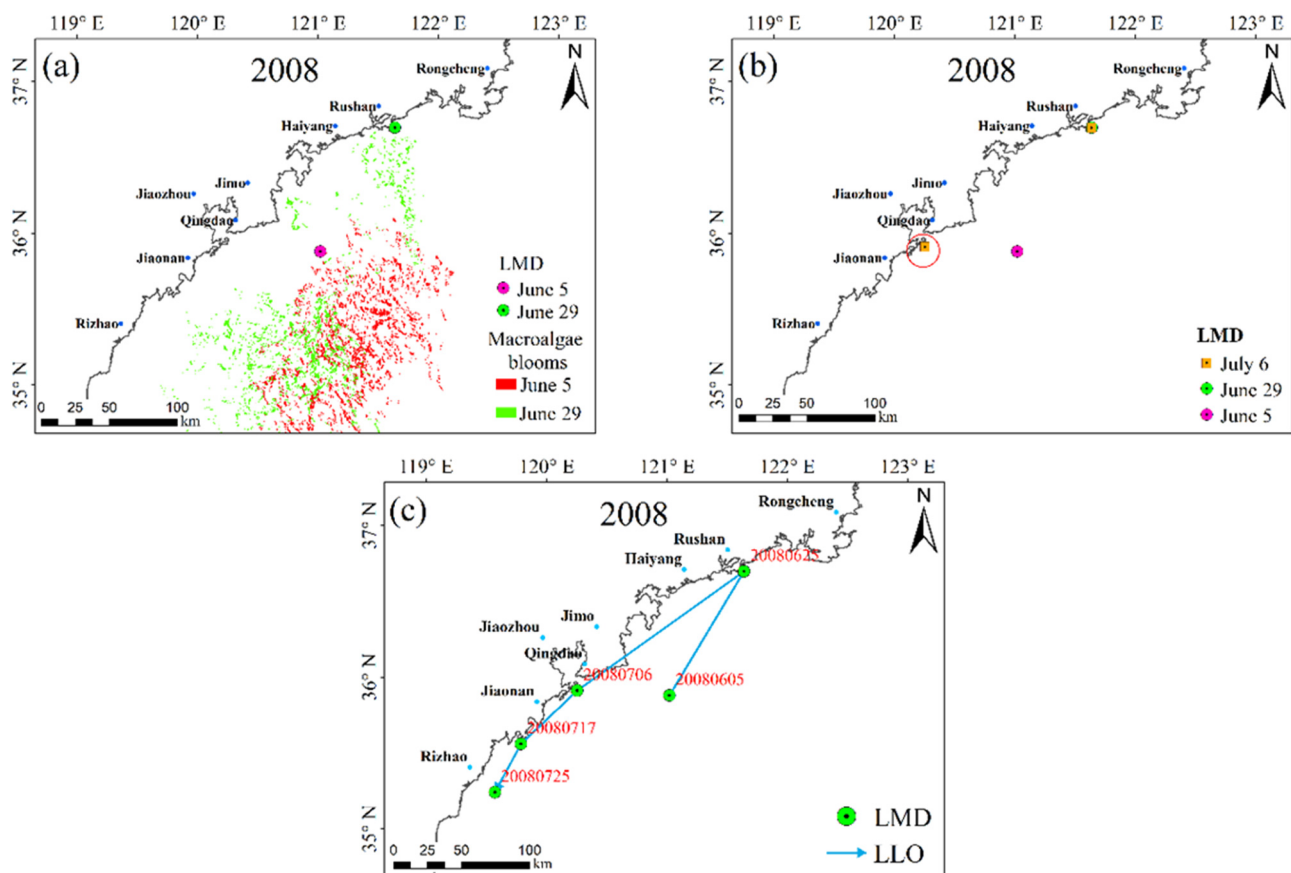


**Figure 4.** (a) Location of minimum distance from offshore (LMD) on 5 June and 29 June 2008. (b) The selection of LMD on 6 July 2008, and the point in red circle is LMD selected on 6 July 2008. (c) The order in which the macroalgae landed in the coastal cities of Shandong Peninsula (LLO) in 2008.

The other characteristic was the degree to which MABs were affecting the southern Yellow Sea, which was represented by distribution density of MABs ( $D_m$ , defined by Equation (7)). To analyze the interannual variation, the annual distribution density ( $ADD$ , defined by Equation (8)) was obtained by calculating the average  $D$  of all images, for every year. The larger the  $ADD$  value, the more serious the degree of effect.

$$D_m = \frac{A_m}{A_s} \times 100\% \quad (7)$$

$$ADD = \frac{\sum_{i=1}^{N_{imgae}} \sum_{m=1}^{N_s} D_m}{N_{imgae}} \quad (8)$$

where  $m$  is the  $m$ th window;  $A_m$  and  $A_s$  are the macroalgae coverage area and the total area of the region in the  $m$ th window, respectively.  $N_s$  is the number of windows in an image, and  $N_{image}$  is the number of selected remote sensing images in each year.

A comparison of  $ADD$  obtained based on a window size of  $2\text{ km} \times 2\text{ km}$ ,  $4\text{ km} \times 4\text{ km}$ , and  $6\text{ km} \times 6\text{ km}$  showed that  $ADD$  has no significant edge variation if a window size is small (Figure 5a). The analysis also showed that the details of  $ADD$  were too rough, especially in regions with a high value of  $ADD$ , if a window size is large (Figure 5c). Therefore, a window size of  $4\text{ km} \times 4\text{ km}$  was selected to calculate  $ADD$ , from 2007 to 2019, because this size could balance the edge variation and presentation of details (Figure 5b).

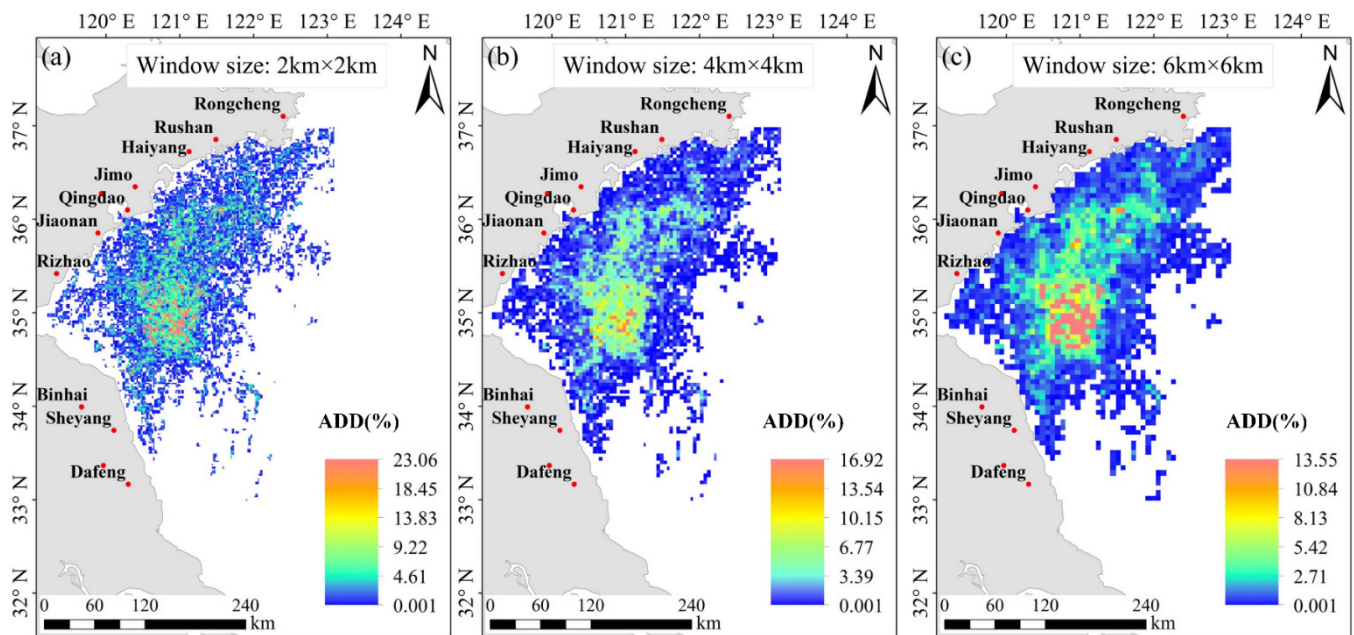


**Figure 5.** Comparison of annual distribution density ( $ADD$ ) of macroalgae blooms based on different window size.

### 3. Results

#### 3.1. Variation in the Macroalgae Daily Dissipation Rate

As shown in Figure 6, we can see the  $DR$  variation characteristics were different in different years. In general, there was an increasing trend with the delay of the starting date in DSE (except in 2010). The TND variation can be divided into the following five types according to the variation trend:

- (1) A general decreasing trend and a maximum value of  $DR$  in the early stage of the dissipation phase, such as in 2010;
- (2) No obvious variation, such as in 2007 and 2011;
- (3) A general increasing trend and a maximum value of  $DR$  in the late stage of the dissipation phase, such as in 2009, 2013, 2014, 2017, 2019 and 2020;
- (4) A trend of TND decreasing at first, then increasing, and decreasing again, such as in 2008, 2012, 2016 and 2018;
- (5) A trend of TND increasing at first, then decreasing, such as in 2015.

Note that the  $DR$  in the 220th day of 2008 and the 202th day of 2012 was not included in the above analysis. The reason was that no suitable fine-resolution images were found before and after these two days, and the mean relative difference (MRD) between  $DR$  calculated by MODIS and  $DR$  calculated by fine-resolution images was relatively larger in the late stage of MAB dissipation phase (Figure 3a,b).

Interestingly, the overall trend in the maximum of  $DR$  was increasing on an interannual scale ( $R^2 = 0.42$ ), which is consistent with  $A_{MAX}$  [14] (Figure 6). It is a manifestation of the effect of the government's macroalgae collecting campaigns in recent years [28].

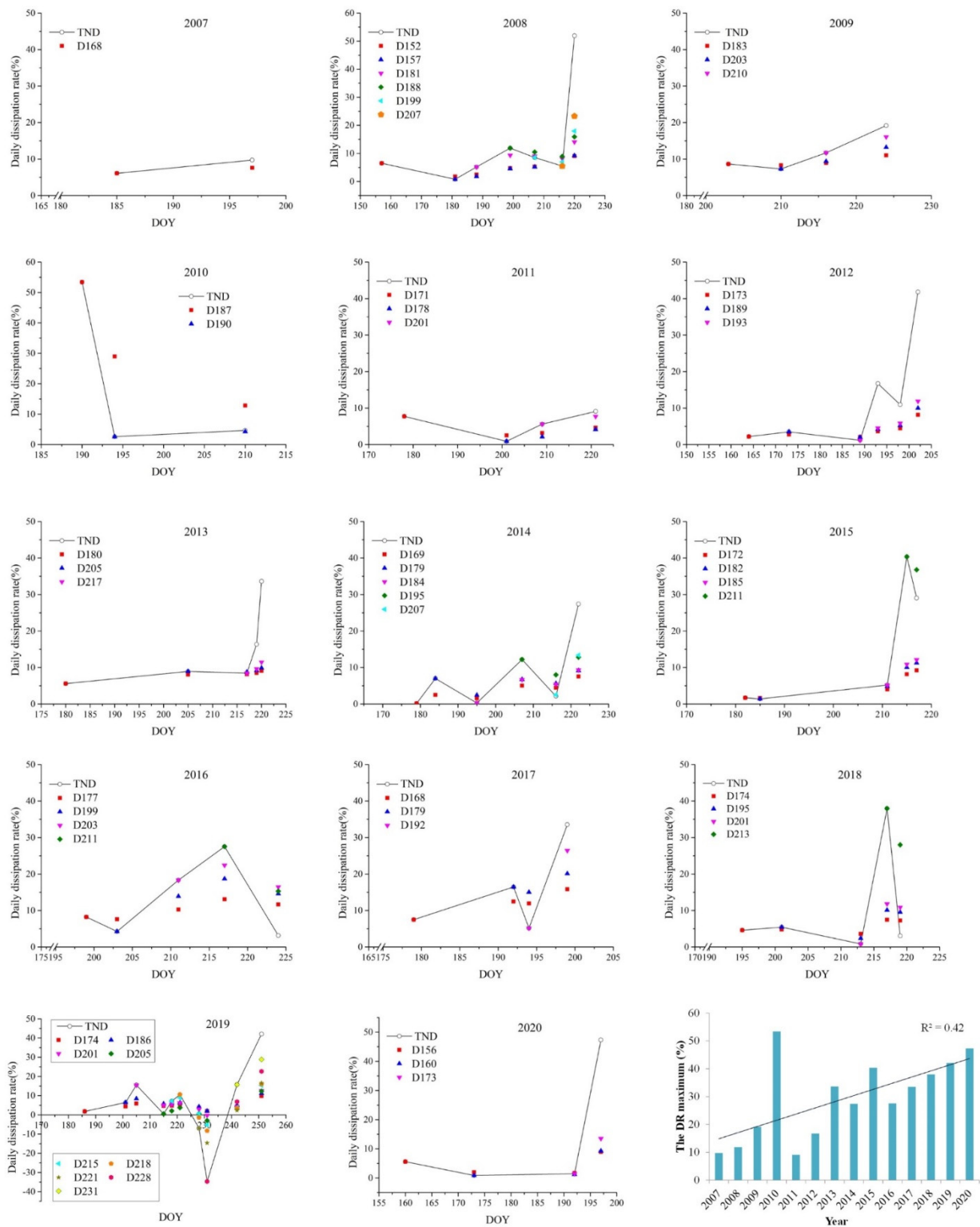


**Figure 6.** Daily dissipation rate (DR) from 2007 to 2020. DOY is day of year. Di represents DR from the same starting date (i) to different ending dates. e.g., ■ D168 in 2007 shows DR with the starting date of 168 (DOY), i.e., 17 June 2007, and the ending date of 16 July 2007. TND is the DR in a period between every two neighboring dates and DSE is the DR calculated during the periods from the same starting date (i) to different ending dates.

### 3.2. The Application of DR Variation: A Simple Method of Estimating Macroalgae Dissipation Days

A simple method of estimating dissipation days for MABs was proposed based on the DR variation from 2007 to 2017. It was then applied to 2018, 2019, and 2020 to determine its reliability. The method is as follows.

- (1) The dissipation phase of MABs was divided into four stages ( $P_1$ – $P_4$ ) according to the annual dissipation days (Figure 7).  $P_1$ – $P_4$  was within 15 days after  $A_{MAX}$ , 16–30 days, 31–45 days, and 46–60 days, respectively.

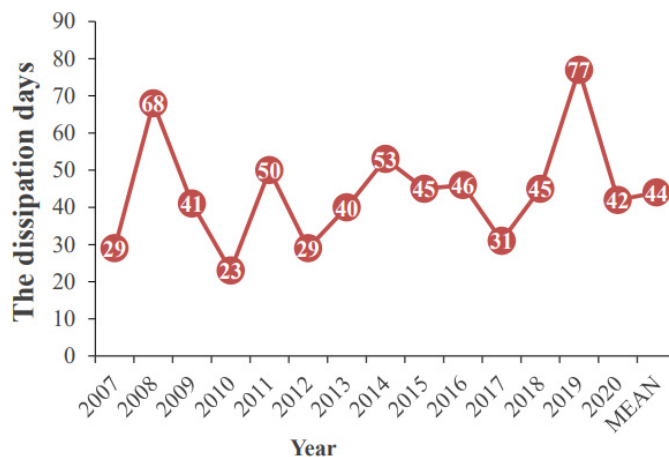


Figure 7. The dissipation days from 2007 to 2020.

- (2) The DSE mean was calculated for each stage that described above from 2007 to 2017, denoted as  $DSE'$ , and the annual mean of  $DSE'$ , denoted as  $ADSE'$  was also calculated. Note that the stage of the year was not included in the calculation if there were no images in that stage.
- (3) The dissipation days for these three years were estimated based on  $A_{MAX}$  for 2018, 2019, and 2020 and  $ADSE'$  of each stage. The detailed process is shown in Figure 8.

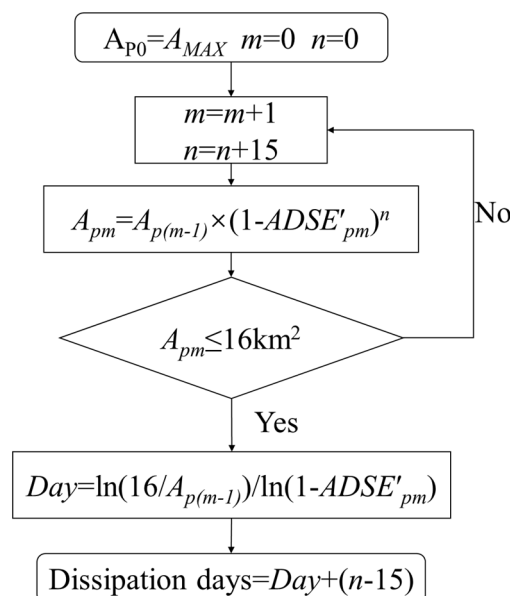


Figure 8. The method of estimating macroalgal blooms (MAB) dissipation days.  $m$  is the  $P_m$  stage, and  $n$  is the  $n$ th day after  $A_{MAX}$ .  $A_{MAX}$  is the maximum of the daily coverage area of MABs.  $A_{pm}$  is the macroalgae daily coverage area on the last day of the  $P_m$  stage.  $ADSE'_{pm}$  is the  $ADSE'$  of the  $P_m$  stage.  $Day$  is the days taken from  $A_{p(m-1)}$  to  $16 \text{ km}^2$ .

Table 1 shows the variation in  $DSE'$  in four stages from 2007 to 2017. It can be seen that  $ADSE'$  in  $P_3$  and  $P_4$  is higher than that in  $P_1$  and  $P_2$ , which is relatively consistent with the  $DR$  variation of each year in Figure 6. Over the 11 years from 2007 to 2017, there were four years in which the maximum of  $DR$  was in  $P_3$  and five years in which the maximum of  $DR$  was in  $P_4$  (as shown in Figure 6).

**Table 1.** Variation of  $DSE'$  in four stages from 2007 to 2017.

Year	$DSE'(\%)$			
	$P_1$	$P_2$	$P_3$	$P_4$
2007	–	7.61	–	–
2008	6.48	0.78	5.19	9.09
2009	–	8.30	13.24	–
2010	28.99	4.64	–	–
2011	7.72	0.88	5.60	9.08
2012	2.19	3.47	4.18	23.47
2013	5.57	–	8.92	11.46
2014	0.17	1.56	12.18	12.80
2015	1.64	–	11.26	–
2016	–	7.62	18.70	3.16
2017	7.50	15.03	33.53	–
$ADSE'$	7.53	5.54	12.53	11.51

The estimation of dissipation days from 2018 to 2020 was close to the actual number of days (Table 2). In 2018 and 2020, the estimated days is consistent with actual days, and the relative error was less than 11.11% between them. For 2019, the relative error may be less than 27.27% if the area variation in the late stage of MAB dissipation phase was the same as the variation in previous years. In general, the dissipation days estimated by the method are relatively consistent with the actual days, indicating that the method is somewhat reliable and accurate.

**Table 2.** Comparison of the estimation of dissipation days and the actual number of days from 2018 to 2020.

Year	$A_{MAX}$ (km <sup>2</sup> )	$n$	MAB Dissipation Days		Actual Days	Relative Error (%)
			Day	Estimation Days		
2018	1493.70	45	5	50	45	11.11
2019	3284.94	45	11	56	77	27.27
2020	640.56	30	13	43	42	2.38

### 3.3. The LLO Variation in MABs Dissipation Phase from 2007 to 2020

The LLO, from 2008 to 2020, is shown in Figure 9. Note that macroalgae were not present in the coastal region of Shandong Peninsula in 2007 based on remote sensing monitoring. It can be seen that the LLO for each year shows obvious variation. The reason for this may be the difference in macroalgae drift trajectory leading to variation in LLO. Previous studies have shown that annual variation in macroalgae drift trajectories is quite high [38]. The LLO was divided into two types. One followed the order of Rizhao, Qingdao, Rushan, and Haiyang, such as during 2010–2014, 2016–2017, and 2020, respectively. The other type was in the reverse order, such as during 2008–2009, 2015, and 2018–2019, respectively. A report titled ‘The Successful Completion of 2019 Green-Tide Defense Mission by the North Sea Department, Ministry of Natural Resources’ published on Chinese Ocean News said that monitoring results by ship and satellite show that in 2019, MABs first affected coastal waters in Weihai and Yantai, i.e., Rongcheng and Haiyang, and then moved to Qingdao and Rizhao. The 2019 LLO in this study was consistent with that report, indicating that the method for determining LLO was reliable.

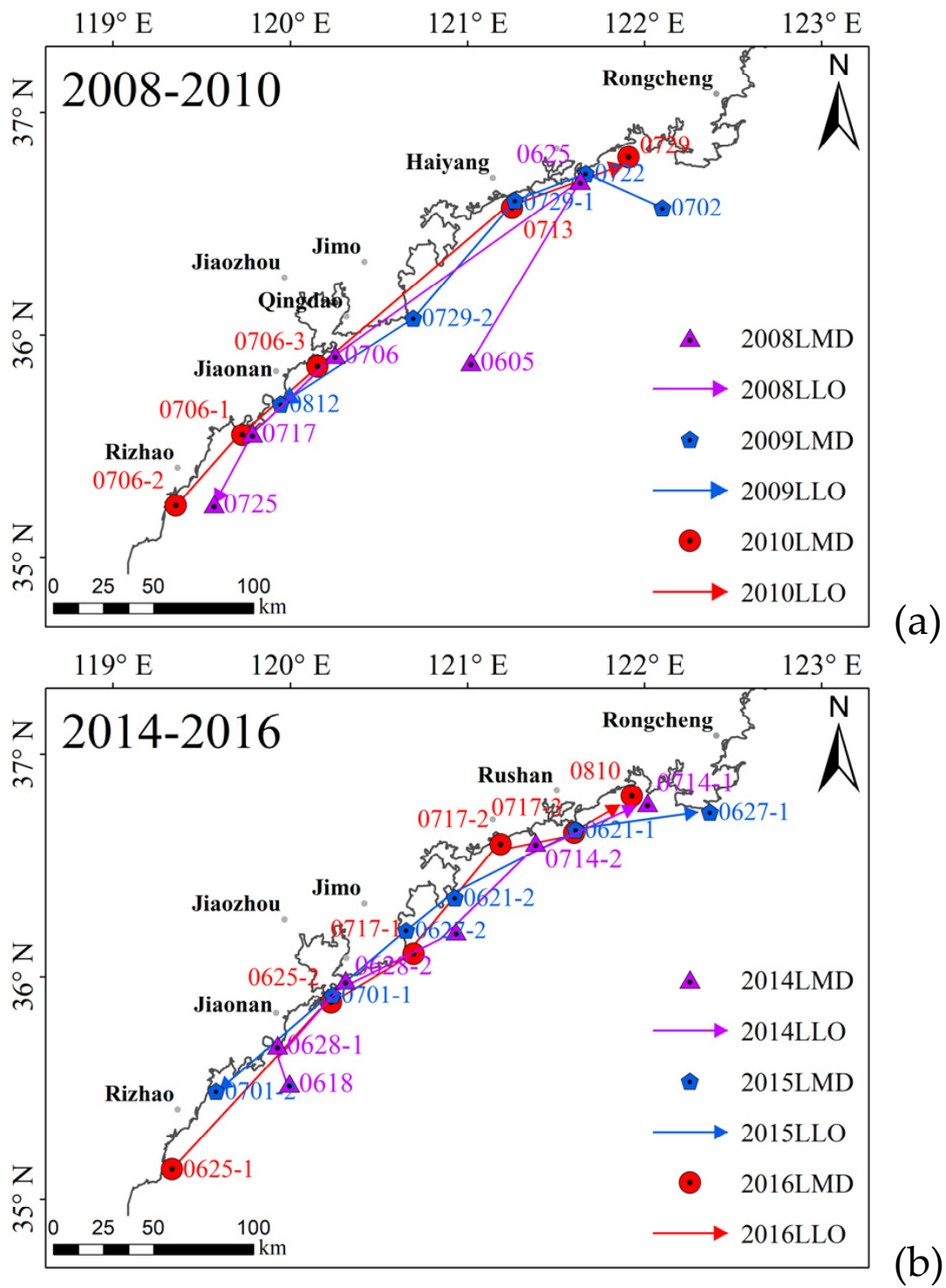
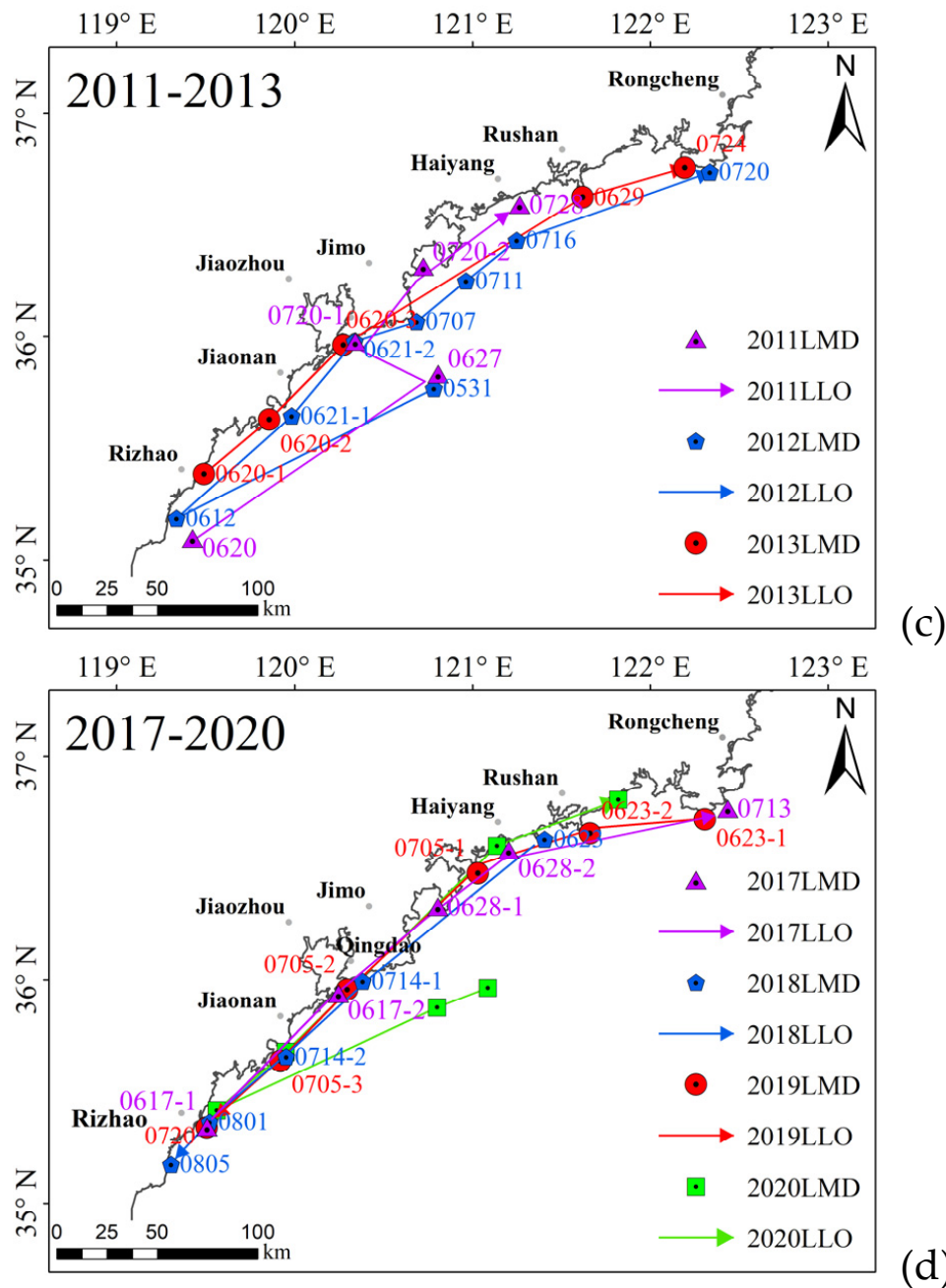


Figure 9. Cont.



**Figure 9.** The LLO variation from 2008 to 2020. The number in figure represents month-date, e.g., 0725 is on July 25. The number after the date is not in sequence.

According to the remote sensing imagery monitoring results, the date on which the macroalgae landed on the entire coastline of Shandong Peninsula was not exactly the same from year to year. The earliest date was 1 July (in 2015) and the latest date was approximately 10 August (in 2009 and 2016). The interval between them was 41 days, illustrating the difficulty of MAB prevention and control in the coastal regions of Shandong Peninsula and reflecting the importance of estimating the dissipation days.

### 3.4. The Annual Distribution Density (ADD) Variation of MABs in the Dissipation Phase

The ADD variation of MABs in the southern Yellow Sea also varied significantly each year due to the difference in the image number, image acquisition time, and the daily macroalgae coverage area (Figure 10). Using the ADD range for each year, the ADDs were divided into five grades to better analyze the interannual variation. The five grades are

(from low to high): L1, L2, L3, L4, and L5. The higher the grade, the higher the *ADD*, and the more serious the effect degree of MABs on this region. An *ADD* above grade L3 is considered a severely affected region. The results are shown in Figure 10. It can be seen the *ADD* was roughly divided into three types according to the distance between the severely affected region and the coastline. The first type was where the severely affected region was distributed in the sea, far from the shore, such as during 2007–2009, 2014, and 2019. The second type was distributed in the coastal waters, such as during 2010–2011 and 2017. The final type was distributed in both coastal waters and the sea, far from the shore, such as during 2012–2013, 2015–2016, 2018, and 2020.

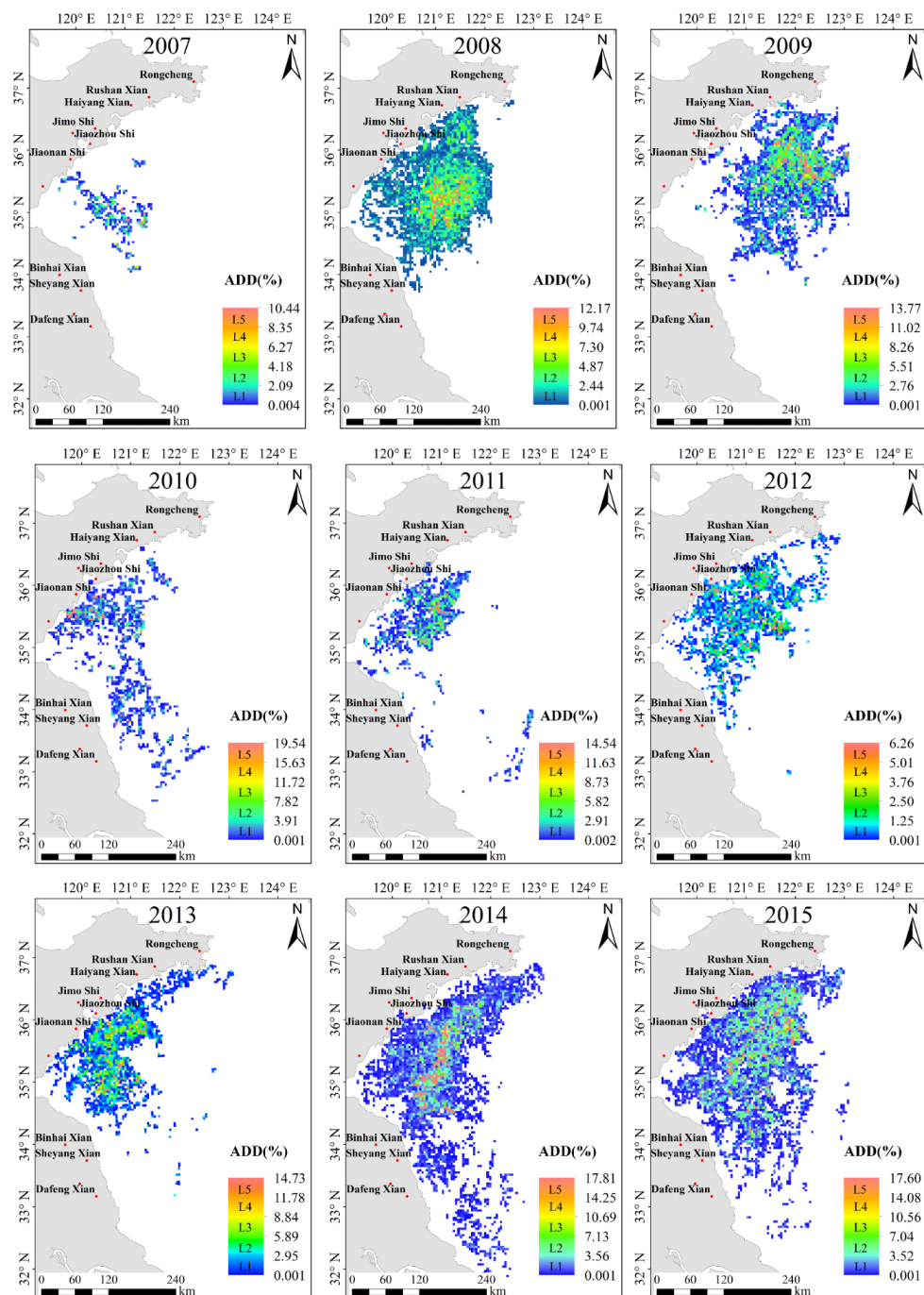
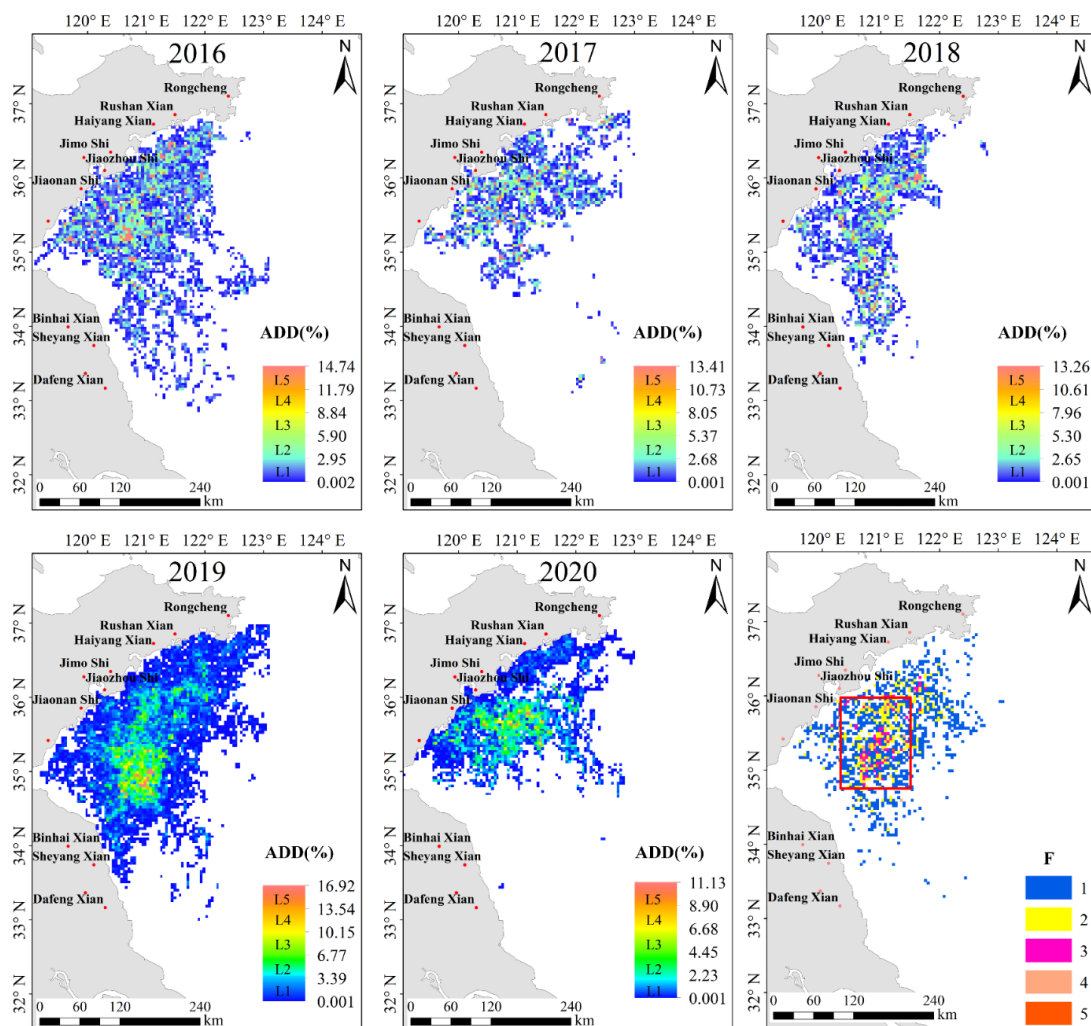


Figure 10. Cont.



**Figure 10.** The annual distribution density of MABs (ADD) on the southern Yellow Sea from 2007 to 2020. The last figure is the coverage frequency of the seriously affected region (F) in these 14 years.

Further analysis of the coverage frequency of the seriously affected region (F) in these 14 years showed that severely affected regions were distributed in the waters north of Sheyang County and south of Rongcheng County. These regions had the highest F value (5), which was caused by differences in ADD and the severely affected region distribution for each year. Small regions were considered the most severely affected regions if their F value were higher than half of the highest F value ( $F \geq 3$ ) in this study. These regions were mostly concentrated in the waters of  $34^{\circ}51'N \sim 36^{\circ}6'N$ ,  $120^{\circ}29'E \sim 121^{\circ}33'E$ .

Given the important economic role of Shandong Peninsula and the requirement for managing MABs, we also analyzed the ADD variation of MABs in the southern Shandong Peninsula coastal waters ( $ADD_{SD}$ ). The results are shown in Figure 11. The variation trend of  $ADD_{SD}$  average in 2007–2020 was decreasing towards northeast and southwest with Qingdao coastal water as the center. In general, there was a slight increasing trend in the  $ADD_{SD}$ , especially in the  $ADD_{SD}$  of Qingdao coastal water ( $R^2 = 0.25$ ,  $p$ -value  $< 0.05$ ). In summary, Qingdao coastal water was the region most seriously affected by MABs on the southern Shandong Peninsula coastal water, and Haiyang coastal water was the second most seriously affected region. Rongcheng coastal water was the least affected, and Rizhao coastal water was the second least affected region.

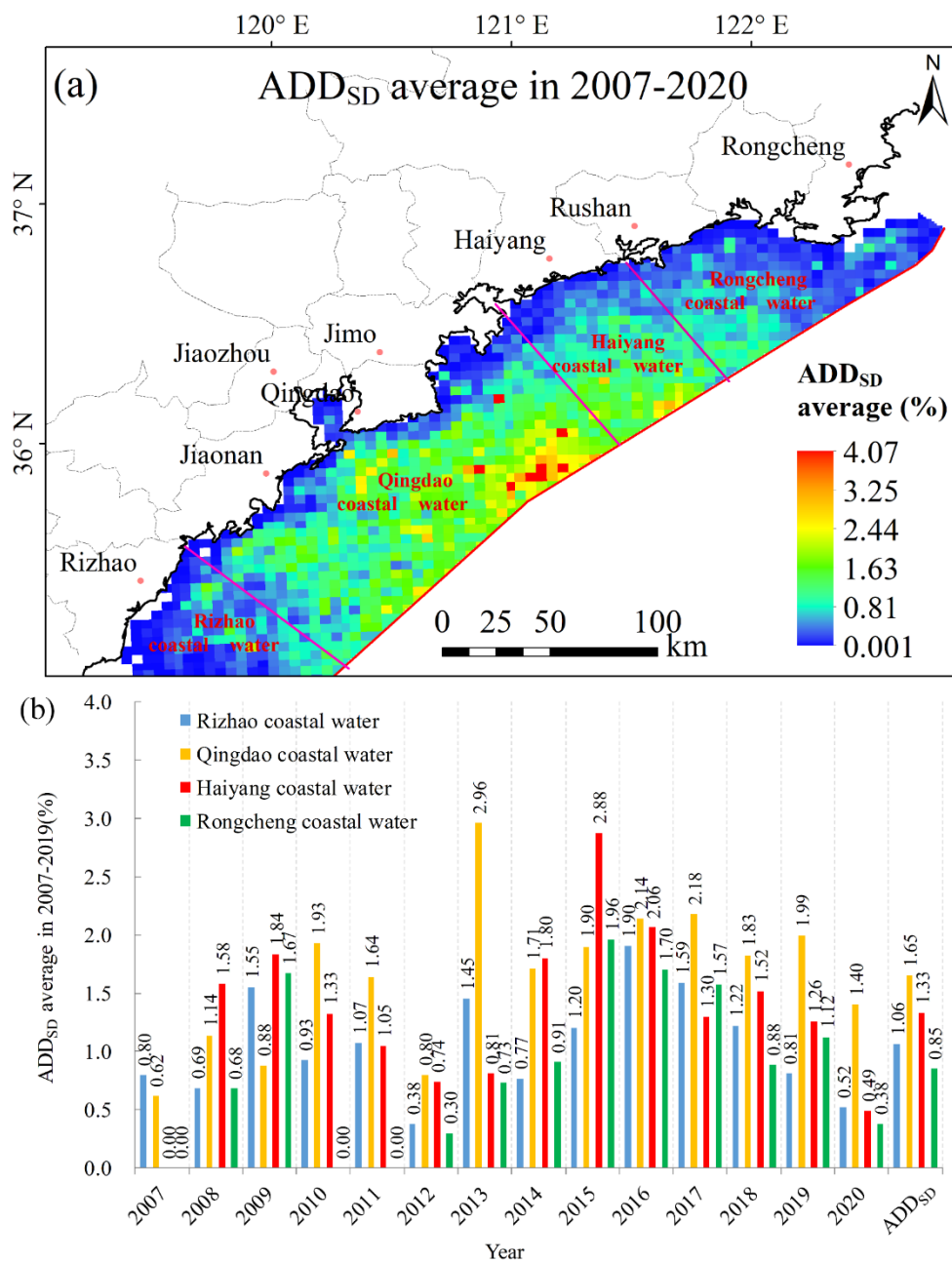


**Figure 11.** The *ADD* variation of MABs on the southern Shandong Peninsula coastal water ( $ADD_{SD}$ ): (a)  $ADD_{SD}$  average in 2007–2020; (b) Interannual variation of  $ADD_{SD}$  on four regions from 2007 to 2020. These four regions were the coastal water of Rizhao, Qingdao, Haiyang and Rongcheng, respectively. *ADD* is the annual distribution density of MABs, and the southern Shandong Peninsula coastal water was determined according to the Marine Function Zone in Shandong Province in this study.

#### 4. Discussion

Because of the limitations of the remote sensing optical images, the *DVI* index we used here only extracts the surface floating macroalgae, and does not consider the distribution of algae in the upper water column, which results in less accurate estimation of the area of coverage, and also leads to some deviation between the *DR* calculated and the actual value. Optical images are seriously affected by the weather, which explains why in some years the interval between two adjacent available images is more than 25 days in this work. In addition, due to macroalgae patch area difference in different regions and stages [11,14,39,40], the stability of linear regression functions among multi-source remote sensing images in Figure 2 needs to be further analyzed and improved. These situations

may cause some deviation from the actual values in the *DR*, *LLO*, and *ADD*. For example, the *LMD* time was later than the actual time in this study. The time of macroalgae first landing in Haiyang was on 17 June 2018 according to the survey of Haiyang macroalgae blooms in 2018 launched by the National Marine Hazard Mitigation Service. However, the time obtained from remote sensing images monitoring was 23 June 2018, 6 days later than the survey time. This disparity can be explained by large amounts of cloud coverage on images acquired before and after June 17.

The variation of *DR*, *LLO*, and *ADD* shows that the spatiotemporal variation of MABs was significantly different from year to year (Figures 6, 9 and 10). It is proved that variations in sea surface winds and surface currents lead to differences in the spatiotemporal variation of MABs [12,17,18,31,41–44]. As shown in Figure 6, the *DR* in 2019 was negative from the 221th day to 231th day (i.e., 9 to 19 August). This period coincides with the LEKIMA typhoon, which changed the environment and the drift trajectory of macroalgae blooms, resulting in an increase in the macroalgae area. This information also indicates that the sea surface winds play an important role in MABs spatiotemporal variation.

## 5. Conclusions

The unique feature of this study is that multiple sensors were used to study the spatiotemporal variation of macroalgae bloom dissipation in the southern Yellow Sea from four aspects including: (1) variation in the daily dissipation rate, (2) variation in the order in which the macroalgae landed in the coastal region of Shandong Peninsula, and (3) variation in the annual distribution density. Our results showed that the spatiotemporal variation differs significantly from year to year. Interestingly, on an interannual scale, the overall trend of the maximum daily dissipation rate is increasing, which is consistent with the maximum of daily coverage area of macroalgae blooms. A simple method of estimating dissipation days of macroalgae blooms is proposed for the first time. The verification results of the method for 2018–2020 show that the estimated dissipation days is relatively consistent with the observed dissipation days obtained from remote sensing images. These spatiotemporal variation features assist in further understanding the macroalgae blooms' dissipation phase, evaluating their ecological and socioeconomic impact, managing the macroalgae collecting campaigns, and providing decision support for relevant departments.

**Author Contributions:** Conceptualization, D.A. and Q.X.; methodology, D.A.; formal analysis, Q.X. and D.A.; writing—original draft preparation, D.A. and Q.X.; writing—review and editing, D.Y., X.Z., Y.Z., L.M. and Q.X. All authors have read and agreed to the published version of the manuscript.

**Funding:** This research was funded by, the National Natural Science Foundation of China (No. 42076188, 41676171, 42106172 and 41911530), the Chinese Academy of Science Strategic Priority Research Program—the Big Earth Data Science Engineering Project (No. XDA1906000, XDA19060203 and XDA19060501), the National Key Research and Development Program of China, grant number 2017YFC1404802, the Key Research and Development Program of Shandong, grant number 2019GHY112017, State Key Laboratory of Tropical Oceanography, South China Institute of Oceanology, Chinese Academy of Sciences, grant number LTO2017, the Natural Science Foundation of Shandong, grant number ZR2019PD021, and the Foundation of Institute of Oceanographic Instrumentation, Shandong Academy of Sciences, grant number HYPY202107.

**Institutional Review Board Statement:** Not applicable.

**Informed Consent Statement:** Not applicable.

**Data Availability Statement:** The data presented in this study are available on request from the corresponding author.

**Acknowledgments:** Thanks to China Center for Resources Satellite Data and Application for providing GF-1 and HJ-1A/1B data, and to NASA's Goddard Space Flight Center and European Space Agency for MODIS and Sentinel-2 data.

**Conflicts of Interest:** The authors declare no conflict of interest.

## References

1. Morand, P.; Merceron, M. Macroalgal Population and Sustainability. *J. Coast. Res.* **2005**, *21*, 1009–1020. [[CrossRef](#)]
2. Smetacek, V.; Zingone, A. Green and golden seaweed tides on the rise. *Nature* **2013**, *504*, 84–88. [[CrossRef](#)]
3. Wang, M.; Hu, C.; Barnes, B.B.; Mitchum, G.; Lapointe, B.; Montoya, J.P. The great Atlantic Sargassum belt. *Science* **2019**, *365*, 83–87. [[CrossRef](#)]
4. Ye, N.H.; Zhang, X.W.; Mao, Y.Z.; Liang, C.W.; Xu, D.; Zou, J.; Zhuang, Z.M.; Wang, Q.Y. ‘Green tides’ are overwhelming the coastline of our blue planet: Taking the world’s largest example. *Ecol. Res.* **2011**, *26*, 477–485. [[CrossRef](#)]
5. Song, X.L.; Huang, R.; Yuan, K.L.; Zhao, Y.H.; Wen, R.B.; Zhang, H.L. Characteristics of the green tide disaster of east Shandong Peninsula offshore. *Mar. Environ. Sci.* **2015**, *34*, 391–395. [[CrossRef](#)]
6. Zhou, M.J.; Liu, D.Y.; Anderson, D.M.; Valiela, I. Introduction to the Special Issue on green tides in the Yellow Sea. *Estuar. Coast. Shelf Sci.* **2015**, *163*, 3–8. [[CrossRef](#)]
7. Hu, C.M. A novel ocean color index to detect floating algae in the global oceans. *Remote Sens. Environ.* **2009**, *113*, 2118–2129. [[CrossRef](#)]
8. Shi, W.; Wang, M.H. Green macroalgae blooms in the Yellow Sea during the spring and summer of 2008. *J. Geophys. Res. Ocean.* **2009**, *114*, C12010. [[CrossRef](#)]
9. Xing, Q.G.; Hu, C.M. Mapping macroalgal blooms in the Yellow Sea and East China Sea using HJ-1 and Landsat data: Application of a virtual baseline reflectance height technique. *Remote Sens. Environ.* **2016**, *178*, 113–126. [[CrossRef](#)]
10. Li, L.; Zheng, X.; Wei, Z.; Zou, J.; Xing, Q. A Spectral-Mixing Model for Estimating Sub-Pixel Coverage of Sea-Surface Floating Macroalgae. *Atmos. Ocean* **2018**, *56*, 296–302. [[CrossRef](#)]
11. Qi, L.; Hu, C.M.; Xing, Q.G.; Shang, S.L. Long-term trend of *Ulva prolifera* blooms in the western Yellow Sea. *Harmful Algae* **2016**, *58*, 35–44. [[CrossRef](#)]
12. Xing, Q.G.; Zheng, X.Y.; Shi, P.; Hao, J.J.; Yu, D.F.; Liang, S.Z.; Liu, D.Y.; Zhang, Y.Z. Monitoring “Green Tide” in the Yellow Sea and the East China Sea Using Multi-Temporal and Multi-Source Remote Sensing Images. *Spectrosc. Spectr. Anal.* **2011**, *31*, 1644–1647. [[CrossRef](#)]
13. Hu, C.; Li, D.; Chen, C.; Ge, J.; Muller-Karger, F.E.; Liu, J.; Yu, F.; He, M.-X. On the recurrent *Ulva prolifera* blooms in the Yellow Sea and East China Sea. *J. Geophys. Res. Oceans* **2010**, *115*. [[CrossRef](#)]
14. Xing, Q.; An, D.; Zheng, X.; Wei, Z.; Chen, J. Monitoring seaweed aquaculture in the Yellow Sea with multiple sensors for managing the disaster of macroalgal blooms. *Remote Sens. Environ.* **2019**, *231*, 111279. [[CrossRef](#)]
15. Cao, Y.Z.; Wu, Y.C.; Fang, Z.X.; Cui, X.J.; Liang, J.F.; Song, X. Spatiotemporal Patterns and Morphological Characteristics of *Ulva prolifera* Distribution in the Yellow Sea, China in 2016–2018. *Remote Sens.* **2019**, *11*, 445. [[CrossRef](#)]
16. Min, S.H.; Oh, H.J.; Hwang, J.D.; Suh, Y.S.; Kim, W. Tracking the Movement and Distribution of Green Tides on the Yellow Sea in 2015 Based on GOCI and Landsat Images. *Korean J. Remote Sens.* **2017**, *33*, 97–109. [[CrossRef](#)]
17. Hu, S.; Yang, H.; Zhang, J.H.; Chen, C.S.; He, P.M. Small-scale early aggregation of green tide macroalgae observed on the Subei Bank, Yellow Sea. *Mar. Pollut. Bull.* **2014**, *81*, 166–173. [[CrossRef](#)] [[PubMed](#)]
18. Son, Y.B.; Choi, B.J.; Kim, Y.H.; Park, Y.G. Tracing floating green algae blooms in the Yellow Sea and the East China Sea using GOCI satellite data and Lagrangian transport simulations. *Remote Sens. Environ.* **2015**, *156*, 21–33. [[CrossRef](#)]
19. Xu, Q.; Zhang, H.Y.; Ju, L.; Chen, M.X. Interannual variability of *Ulva prolifera* blooms in the Yellow Sea. *Int. J. Remote Sens.* **2014**, *35*, 4099–4113. [[CrossRef](#)]
20. Fan, S.; Fu, M.; Wang, Z.; Zhang, X.; Song, W.; Li, Y.; Liu, G.; Shi, X.; Wang, X.; Zhu, M. Temporal variation of green macroalgal assemblage on *Porphyra* aquaculture rafts in the Subei Shoal, China. *Estuar. Coast. Shelf Sci.* **2015**, *163*, 23–28. [[CrossRef](#)]
21. Huo, Y.; Han, H.; Shi, H.; Wu, H.; Zhang, J.; Yu, K.; Xu, R.; Liu, C.; Zhang, Z.; Liu, K. Changes to the biomass and species composition of *Ulva* sp. on *Porphyra* aquaculture rafts, along the coastal radial sandbank of the Southern Yellow Sea. *Mar. Pollut. Bull.* **2015**, *93*, 210–216. [[CrossRef](#)]
22. Liu, D.; Keesing, J.K.; Xing, Q.; Ping, S. World’s largest macroalgal bloom caused by expansion of seaweed aquaculture in China. *Mar. Pollut. Bull.* **2009**, *58*, 888–895. [[CrossRef](#)]
23. Liu, X.; Li, Y.; Wang, Z.; Zhang, Q.; Cai, X. Cruise observation of *Ulva prolifera* bloom in the southern Yellow Sea, China. *Estuar. Coast. Shelf Sci.* **2015**, *163*, 17–22. [[CrossRef](#)]
24. Zhang, J.; Huo, Y.; Wu, H.; Yu, K.; Kim, J.K.; Yarish, C.; Qin, Y.; Liu, C.; Ren, X.; He, P. The origin of the *Ulva* macroalgal blooms in the Yellow Sea in 2013. *Mar. Pollut. Bull.* **2014**, *89*, 276–283. [[CrossRef](#)]
25. Zheng, X.Y.; Xing, Q.G.; Li, L.L.; Shi, P. Numerical simulation of the 2008 green tide in the Yellow Sea. *Mar. Sci.* **2011**, *35*, 82–87.
26. Huo, Y.; Han, H.; Hua, L.; Wei, Z.; Yu, K.; Shi, H.; Kim, J.K.; Yarish, C.; He, P. Tracing the origin of green macroalgal blooms based on the large scale spatio-temporal distribution of *Ulva* microscopic propagules and settled mature *Ulva* vegetative thalli in coastal regions of the Yellow Sea, China. *Harmful Algae* **2016**, *59*, 91–99. [[CrossRef](#)] [[PubMed](#)]
27. Song, W.; Li, Y.; Fang, S.; Wang, Z.; Xiao, J.; Li, R.; Fu, M.; Zhu, M.; Zhang, X. Temporal and spatial distributions of green algae micro-propagules in the coastal waters of the Subei Shoal, China. *Estuar. Coast. Shelf Sci.* **2015**, *163*, 29–35. [[CrossRef](#)]
28. Xing, Q.; Wu, L.; Tian, L.; Cui, T.; Wu, M. Remote sensing of early-stage green tide in the Yellow Sea for floating-macroalgae collecting campaign. *Mar. Pollut. Bull.* **2018**, *133*, 150–156. [[CrossRef](#)] [[PubMed](#)]
29. Wang, Z.; Xiao, J.; Fan, S.; Li, Y.; Liu, X.; Liu, D. Who made the world’s largest green tide in China?—An integrated study on the initiation and early development of the green tide in Yellow Sea. *Limnol. Oceanogr.* **2015**, *60*, 1105–1117. [[CrossRef](#)]

30. Wei, Q.; Wang, B.; Yao, Q.; Fu, M.; Sun, J.; Xu, B.; Yu, Z. Hydro-biogeochemical processes and their implications for *Ulva prolifera* blooms and expansion in the world's largest green tide occurrence region (Yellow Sea, China). *Sci. Total Environ.* **2018**, *645*, 257–266. [[CrossRef](#)]
31. Xu, Q.; Zhang, H.; Cheng, Y.; Zhang, S.; Wei, Z. Monitoring and Tracking the Green Tide in the Yellow Sea With Satellite Imagery and Trajectory Model. *IEEE J. Sel. Top. Appl. Earth Obs. Remote Sens.* **2017**, *9*, 5172–5181. [[CrossRef](#)]
32. Xing, Q.G.; Hu, C.M.; Tang, D.L.; Tian, L.Q.; Tang, S.L.; Wang, X.H.; Lou, M.J.; Gao, X.L. World's Largest Macroalgal Blooms Altered Phytoplankton Biomass in Summer in the Yellow Sea: Satellite Observations. *Remote Sens.* **2015**, *7*, 12297–12313. [[CrossRef](#)]
33. Li, L.; Xing, Q.; Li, X.; Yu, D.; Zhang, J.; Zou, J. Assessment of the Impacts From the World's Largest Floating Macroalgae Blooms on the Water Clarity at the West Yellow Sea Using MODIS Data (2002–2016). *IEEE J. Sel. Top. Appl. Earth Obs. Remote Sens.* **2018**, *11*, 1397–1402. [[CrossRef](#)]
34. Wu, X.Q.; Xu, K.D.; Yu, Z.S.; Yu, T.T.; Lei, Y.L. Standing crop and spatial distribution of meiofauna in Yellow Sea at late stage of *Enteromorpha prolifera* bloom in 2008. *Chin. J. Appl. Ecol.* **2010**, *21*, 2140–2147. [[CrossRef](#)]
35. Tq, A.; Xz, A.; Yh, A.; Yi, Z.A.; Chen, G.A.; Ch, A.; Xta, B.; Ying, W. Ecological effects of *Ulva prolifera* green tide on bacterial community structure in Qingdao offshore environment. *Chemosphere* **2020**, *244*, 125477. [[CrossRef](#)]
36. Wang, X.H.; Li, L.; Bao, X.; Zhao, L.D. Economic Cost of an Algae Bloom Cleanup in China's 2008 Olympic Sailing Venue. *Eos Trans. Am. Geophys. Union* **2013**, *90*, 238–239. [[CrossRef](#)]
37. Cui, T.W.; Liang, X.J.; Gong, J.L.; Tong, C.; Xiao, Y.F.; Liu, R.J.; Zhang, X.; Zhang, J. Assessing and refining the satellite-derived massive green macro-algal coverage in the Yellow Sea with high resolution images. *ISPRS J. Photogramm. Remote Sens.* **2018**, *144*, 315–324. [[CrossRef](#)]
38. Guo, W.; Zhao, L.; Li, X.M. The interannual variation of Green Tide in the Yellow Sea. *Haiyang Xuebao* **2016**, *38*, 36–45. [[CrossRef](#)]
39. Xiao, Y.F.; Zhang, J.; Cui, T.W. High-precision extraction of nearshore green tides using satellite remote sensing data of the Yellow Sea, China. *Int. J. Remote Sens.* **2017**, *38*, 1626–1641. [[CrossRef](#)]
40. Hu, L.B.; Zeng, K.; Hu, C.M.; He, M.X. On the remote estimation of *Ulva prolifera* areal coverage and biomass. *Remote Sens. Environ.* **2019**, *223*, 194–207. [[CrossRef](#)]
41. Jian, L.U.; Zhang, Q.L.; An-Chun, L.I. The influence of Subei coastal current on the outbreak and drift of *Enteromorpha prolifera*. *Mar. Sci.* **2014**, *10*, 83–89. [[CrossRef](#)]
42. Lee, J.H.; Pang, I.-C.; Moon, I.-J.; Ryu, J.-H. On physical factors that controlled the massive green tide occurrence along the southern coast of the Shandong Peninsula in 2008: A numerical study using a particle-tracking experiment. *J. Geophys. Res. Oceans* **2011**, *116*. [[CrossRef](#)]
43. Zhang, S.P.; Liu, Y.C.; Zhang, G.Q.; Lei, G. Analysis on the Hydro-Meteorological Conditions from Remote Sensing Data for the 2008 Algal Blooming in the Yellow Sea. *Period. Ocean Univ. China* **2009**, *39*, 870–876. [[CrossRef](#)]
44. Wang, Z.; Fu, M.; Jie, X.; Zhang, X.; Wei, S. Progress on the study of the Yellow Sea green tides caused by *Ulva prolifera*. *Haiyang Xuebao* **2018**, *40*, 1–13. [[CrossRef](#)]